Feasibility Study of an All-Electric 150 Passenger Aircraft

Gregory G. Zilliac, Jeffrey V. Bowles, Robert K. Fong, Michael J. Schuh
and Dahlia D.V. Pham
NASA Ames Research Center, Moffett Field, CA, USA

Vladimir Kuptsov
MotorXP LLC, Chino, CA

Among the potential future technologies for low-carbon transport aircraft, all-electric concepts stand out environmentally, yet their feasibility and cost-effectiveness at scale remain uncertain. **This paper examines the conceptual design of an all-electric 150-passenger aircraft with a range of 840 NM based on assumed future battery cell-level specific energy of 1330 Wh/kg. The tube and wing design is propelled by open rotors driven by four electric motors per nacelle and utilizes advanced structural materials for weight reduction. Powertrain technology gaps are identified. The conceptual design shows that all-electric aviation could supplant about 30% of current fossil fuel use by transport aircraft and potentially more with air-traffic-control modifications.**

I. Nomenclature

A	Rotor annulus area
AC	Alternating current
C	Battery cell charging or discharging rate
C_P	Power coefficient
C_T	Thrust coefficient
CR	Counter rotating variable pitch open rotor
CAFFI	Commercial *Aviation* Alternative Fuels Initiative
CFM	CFM International is a General Electric and Safran joint venture
CLEEN	Continuous Lower Energy, Emissions, and Noise
D	Rotor tip diameter (of forward rotor for CR)
DC	Direct current
D_{cmil}	Conductor diameter in circular mil
DRM	Design Reference Mission
E	Energy or rate of battery energy charging or discharging
EPFD	NASA Electrified Powertrain Flight Demonstrator
EV	Electric Vehicle
f	Frequency, Hz.
FAA	Federal Aviation Administration
GASP	General Aviation Synthesis Program
GHG	Greenhouse Gas
IATA	International Air Transport Association
ICAO	International Civilian Aviation Organization
IFR	Instrument Flight Rules
IGBT	Insulated-Gate Bipolar Transistor
J	Rotor advance ratio
Li-ion	Lithium-ion battery
MOSFET	Metal–Oxide–Semiconductor Field-Effect Transistor
MSY	New Orleans airport code

n	Rotor revolutions per second
N_{motors}	Total number of motor poles
N_{packs}	Total number of battery packs
N_p	Number of motor poles
NOx	Oxides of Nitrogen
ORD	Chicago O'hare airport code
P	Power
PAX	Number of Passengers
PQAJ3	Rotor power loading parameter
Q	Torque
RISE	Revolutionary Innovation for Sustainable Engines
rms	Root mean square
rpm	Revolutions Per Minute
SABERS	Solid-state Architecture Batteries for Enhanced Recharge ability and Safety
Shp	Shaft horsepower
SiC	Silicon Carbide *(*SiC*)* MOSFET
SFD	NASA Sustainable Flight Demonstrator
SLS	Standard sea level
SR	Single variable pitch open rotor
SSLB	Solid State Lithium Battery
SUGAR	Subsonic Ultra Green Aircraft Research
SUSAN	SUbsonic Single Aft eNgine
T	Thrust
TTBW	Transonic Truss Braced Wing
V	Velocity
VP	Variable pitch
β	Blade angle (subscript F:forward, A:aft)
η	Efficiency
ρ	Air density
ϕ	Angle between the apparent and real power in the vector space power triangle

II. Introduction

The Federal Aviation Administration (FAA) recently published the United States 2021 Aviation Climate Action Plan[1] that sets a goal of net-zero greenhouse gas (GHG) emissions from the U.S. aviation sector by 2050. Considering today's technology and resources projected into the future, only the most optimistic projections achieve net-zero GHG by 2050. The U.S. plan relies heavily on sustainable aviation fuels (SAF) which can be produced carbon neutrally, but the fuels emit water vapor when burned resulting in contrails at altitude that contribute substantially to global warming. Furthermore, the plan deemphasizes the possibility of all-electric aviation as a net-zero solution prior to 2050. Is all-electric aviation in the solution space post 2050? A recent study[2] showed that if an all-electric single aisle 150-passenger aircraft with a mission range of 840 NM was feasible, it could service nearly 50% of all U.S. departures and would lead to a reduction of 29% in aviation fuel consumed annually based on current demand.

An all-electric 150 passenger aircraft is not feasible today. The primary stumbling point is that the energy density of suitable commercially available batteries or other power storage technologies is too low by a factor of at least four to five to be viable. The lithium-ion cells, currently used in cars and small airplanes, have a cell-level specific energy of approximately 300 Wh/kg which is too low for other than short hops with low passenger counts. Furthermore, lithium-ion cells can form lithium dendrites that can short circuit a cell and lead to fires (e.g. Eviation Alice prototype fire in 2020) and so the safety level of the current generation of these cells is insufficient for use in large quantities on aircraft.

The short fall in battery specific energy has led designers to consider SAF/electric hybrid aircraft propulsion concepts to reduce fossil fuels consumption. In 2009, Boeing proposed SUGAR Volt, a 154-passenger transonic truss-braced wing hybrid-electric concept that purportedly will reduce fuel consumption by up to 79 percent in comparison

to a baseline aircraft for a 900 NM mission. Later studies by Boeing showed that hybridized tube and wing concepts could achieve nearly the same fuel savings[3].

Another promising hybrid concept is SUSAN[4] a 180-passenger aircraft with a 750-mile economic range and a 2,500-mile design range that implements a single gas turbine generator/thruster and an array of 1 MW electric motors distributed along the wing. SUSAN would operate within the existing airport infrastructure and has the potential to reduce aircraft emissions by 50% per passenger-mile while retaining the size, speed and range of large regional jets.

Currently, GE Aviation and magniX are developing hybrid-electric flight demonstrators as part of NASA's Electrified Powertrain Flight Demonstrator (EPFD) program. GE Aviation in partnership with Boeing are working on a hybrid-electric powertrain implemented on the SAAB 340B turboprop airframe. Initially, they plan to add a motor/generator in line with one of the two CT7 engines and demonstrate a hybrid-electric system in flight from 10,000 ft to 30,000 ft. In a similar effort, magniX plans to hybridize a DeHavilland Canada Dash 7 turboprop aircraft by replacing two of the four PT6A-50 turboprops engines with magniX magni650 electric propulsion units. The technology developed and evaluated as part of these EPFD supported demonstrations will be invaluable.

In the short run, concepts that rely on SAF will result in net CO_2 reduction. The big question is whether there is enough biomass to support SAF production at the scale needed by aviation in the future. The position of CAFFI, a coalition of SAF stakeholders, is that enough U.S. biomass exists in the form of wastes, fats, oils, greases, gases, and residues to produce 15.6 billion gallons of jet fuel per year in the U.S. (about 59% of the 2018 U.S. demand[5]). Worldwide, 410 Mt of biomass is believed to be available which is enough to meet 120% of projected 2030 jet fuel demand[6]. Even if SAF production at scale is feasible, biomass feed stock would be better put to use fueling diesel engines in trucks, rail and ships because the GHG benefit would be the same but the cost of producing the diesel fuel would be substantially less than producing SAF. Furthermore, it is generally believed that use of biomass-derived fuels will need to be coupled with carbon capture technologies to achieve carbon neutrality.

On the all-electric aircraft front, the technology challenges are formidable. Wright Electric Inc. of Albany, New York has proposed the Wright 1, a 186-passenger, 800 NM range all-electric aircraft driven by an array of 2 MW (2,700 hp) electric motors that are currently being tested. Wright is also developing the Spirit, a 100-passenger all-electric, zero-emissions aircraft based on the BAe 146 airframe with a flight time of up to one hour.

Other notable all-electric aircraft concepts with reasonable passenger counts and range include VoltAir and Ce-Liner. In 2011, Airbus proposed the VoltAir, a 68 PAX aircraft with a range of 900 NM, using 1000 Wh/kg Lithium-air batteries[7]. A single aft-ducted fan propels the sleek looking low-drag concept. During the same timeframe as Voltair, Ce-Liner proposed a 189 pax concept that uses advanced lithium ion battery technology (assumed to be 2000 Wh/kg) and a C-wing planform was proposed by Bauhaus Luftfahrt, an aviation think tank from Germany[8]. Both Voltair and Ce-liner do not appear to have progressed beyond the conceptual design phase.

A pair of recent top-level studies[9,10] of all-electric aircraft using distributed propulsors conclude that a 120 pax battery-electric aircraft with a cruise range of 1000 km (300 km reserve range provided by a SAF-fueled gas turbine), is feasible, assuming a usable battery energy density of 300 Wh/kg.

When considering electrifying aircraft from an overall energy point of view, electric propulsion is roughly twice as efficient in comparison to the thermally driven counterparts. Because of the low specific energy levels of electricity storage in comparison to the energy stored in a gallon of Jet A, electric aircraft are inherently heavier. Sustainably produced electricity is a fraction of the cost of jet fuel based on useable energy (even when taking into account the cost of new production and distribution).[11] Optimistically, we are one major battery breakthrough away from large scale electric powered aviation becoming technically feasible. Hopefully, the pace of technology development will outstrip the pace of global warming.

In this paper we consider the feasibility of a notional all-electric aircraft design (based on an assumed battery specific energy of 1330 Wh/kg) that could have a significant impact on GHG emissions and NOx pollutants by aviation in the future. Feasibility, sustainability and GHG reduction drive the design choices while cost and performance are secondary considerations. Where necessary, technology projections are made and technology gaps are pointed out.

III. Analysis

A. Design Reference Mission

Shown in figure 1 is a histogram of aviation fuel used in the U.S. in 2020 binned by fight distance based on data from the Sherlock database combined with the International Civil Aviation Organization (ICAO) fuel consumption model[2]. As one might expect, there is no obvious delineation between flight distances that would best be served by electric aircraft and the longer range flights that would rely on SAF or potentially hydrogen. For this study, we have chosen a design reference mission (DRM) range of 840 NM and a passenger count of 150 because this is envisioned as the upper bound of what could be technically feasible post 2050 for all-electric transports. An aircraft with this capability would replace 66% of all U.S. flight departures (based on the 2020 departure counts). As a point of reference, the DRM of 840 NM represents a Boeing 737-800 flight between Chicago and New Orleans.

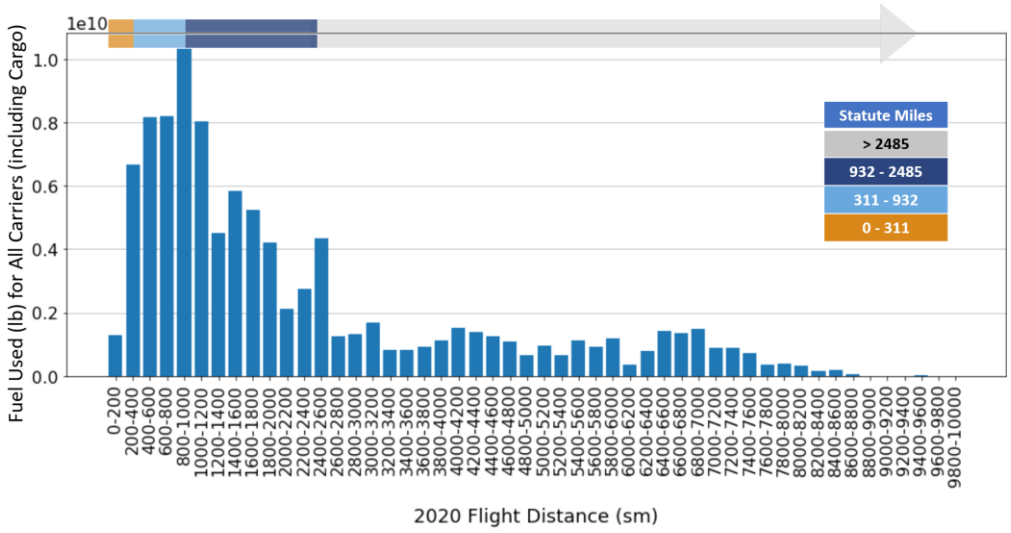

Figure 1. Histogram of fuel used in 2020 by distance in 200-statute mile increments (adapted from ref. 2).

The DRM modeled is depicted in figure 2. Included in the DRM are energy reserves required by Part 121.639 of the U.S. Code of Federal Regulations in the event of a missed approach followed by flight to an alternate airport 100 NM away plus sufficient energy to cruise for 45 minutes at normal cruise power. As will be shown the total reserve energy required for this mission is substantial (≈ 24.5% of the total onboard energy). It should be noted that additional reserves beyond that included in the DRM are required to account for adverse winds and weather.

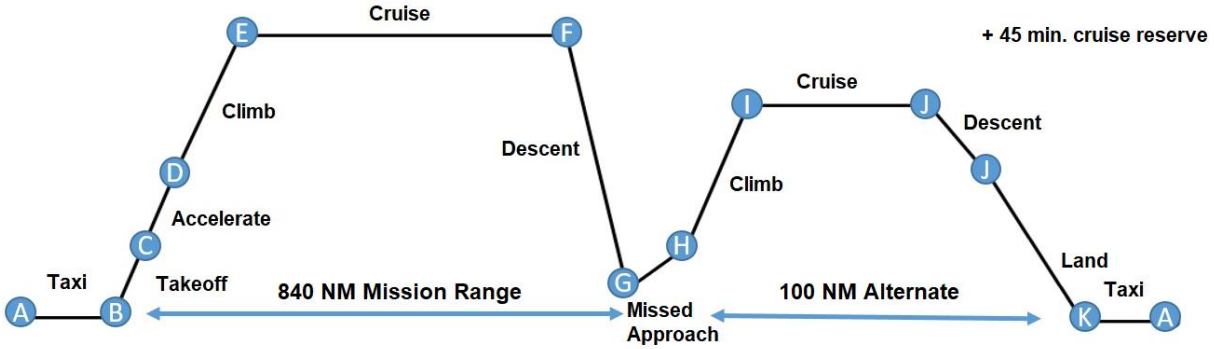

Figure 2. Design reference mission profile including Part 121 reserves.

For transport all-electric aircraft designs, the most limiting design constraint is the takeoff critical engine out 2nd segment minimum climb performance requirement of 14 CFR 25 §25.121 that requires a climb gradient greater than 2.4% for one of two-engines out. Essentially, this requirement sizes the motor.

B. Efficiency and Power Factor

In the following sections, efficiency defined as $\eta_{component} = P_{out}/P_{in}$ is discussed. Considered are efficiencies associated with the battery, DC cabling, inverter, AC cabling, gearbox, motor and rotor. The following relationship shows how the efficiencies stack up:

$$P_{motor\_SHP} \times 746 = P_{bat\_in\_dc}\eta_{battery}\eta_{cable}\eta_{inv}\eta_{gear}\eta_{motor} \quad \text{(W)}$$
$$\eta_{cable} = \eta_{ac\_cable}\eta_{dc\_cable}$$

Unlike gas turbines, electric motors can be designed to efficiently produce torque at shaft rotation rates that match rotor high-efficiency advance ratios and therefore a gearbox between the motor and rotor should not be required (modeled as $\eta_{gear} = 1.0$). The efficiency associated with the thrust power produced by the propeller is:

$$\eta_{net} = \frac{TV}{P_{motor\_SHP} \times 746}$$

In the simulation, all of the efficiencies multiply together and so a total efficiency is defined as:

$$\eta_{total} = \eta_{battery}\eta_{cable}\eta_{inv}\eta_{gear}\eta_{motor}\eta_{net}$$

The power consumed by the star-connected three-phase motor is:

$$P_{motor\_in\_rms} = 3V_{phase\_rms}I_{phase\_rms}PF$$

Where *PF* is the power factor of the motor caused by the presence of reactive power within the motor. The power factor is ≈0.95 during cruise and lower during takeoff and climb. The power factor alters the phase current levels required to produce the desired shaft power but it does not impact the overall power consumed from the battery. Power factor does impact the AC cabling efficiency because it, along with the elevated inverter-produced AC frequency levels and resistive losses, increase the AC cable effective impedance.

C. Energy Storage

The bulk of the analysis in this paper is independent of a particular onboard energy storage technology. It is assumed that the volumetric energy storage density is 1000 Wh/L and a range of stored gravimetric specific energy levels between 1000 and 2600 Wh/kg are explored. Nevertheless, batteries are the most likely energy storage medium for future electric aviation. The ideal battery for aviation has high specific energy, high energy density, can be rapidly charged and discharged, is safe, sustainable and cost effective. Unfortunately, no such battery exists today. The most promising battery technology on the near horizon are solid-state lithium batteries.

Battery specific energy level projections based on the electro-chemistry theoretical upper limits and the historical specific energy-growth-rate trends for several battery chemistries are show in figure 3 (figure from reference 12). If these projections hold true, the all-electric 150 pax DRM will not be possible until after 2070 because, as will be shown, a specific energy level of at least 1330 Wh/kg is required for the 840 NM DRM. For reference, the specific energy of Jet-A fuel is 11,990 Wh/kg.

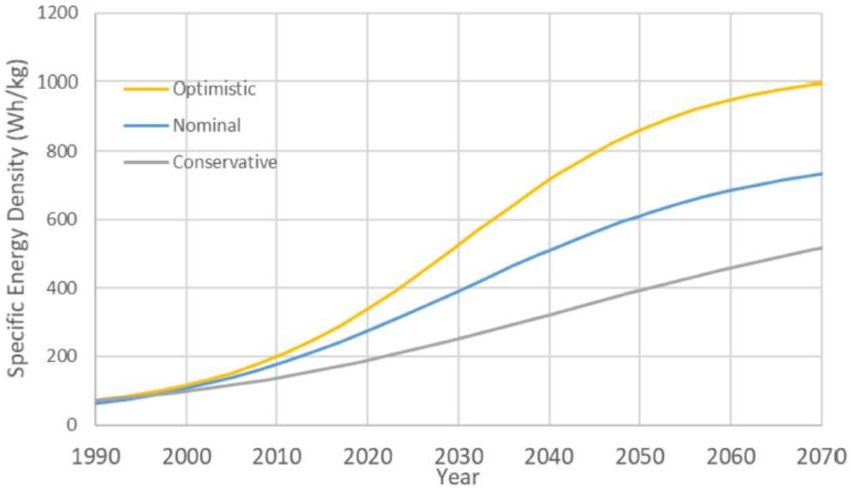

Figure 3. Project battery specific energy levels (from ref 12).

Currently, dozens of companies are working on Solid State Lithium Battery (SSLB) technologies and battery chemistry. Battery form factor and pack design are also evolving. An example of one SSLB development effort by NASA and collaborators is SABERS[13] that uses a stacked flat cell configuration resulting in lab-bench-tested specific energy of up to 1100 Wh/kg (when discharged at 0.4C). It is expected that the cell level energy density of SSLBs will be greater than 1000 Wh/L. The open cell voltage of SSLBs is quite high ranging between 3.0 and 4.9 volts depending on the specifics of the cell design. Unfortunately, manufacturers are still in the prototype stage and therefore have not produced products with published datasheets.

One of the chief attributes of SSLBs is their safety. The solid electrolyte used in these batteries does not sustain growth of dendrites and therefore the fire hazard likelihood of SSLBs is lower than their Li-ion counterpart. Additionally, these batteries can be rapidly charged and discharged, can operate from -20C to 100C, and some can be recharged up to 10,000 times at a rate of 20C with 82% capacity retention[14]. Another significant advantage over many battery technologies is that SSLB packs do not require as substantial of a thermal management systems in comparison to Li-ion (because they are more efficient). A key advantage of SSLBs for aviation is they can be deeply discharged to near zero without damaging the cells (unlike Li-ion where the minimum state-of-charge limit is 5 to 20%).

The claim is that SSLBs can be safely recycled but the current recycling rate of Li-ion batteries is only 5% in the U.S. and so it remains to be seen if the recycling rate SSLBs is higher once they are produced in large quantities. Recycling of the lithium is critical to the success of lithium-based batteries because chronic lithium shortages are expected post 2030. Some SSLBs use rare and expensive metals like cobalt and nickel that researchers hope to eliminate.

Numerous design and manufacturing challenges remain before the SSLB will find widespread use. Solid-state battery cells expand when charging and shrinks when discharging which complicates the cell and pack design. Finally, the manufacturing process of SSLBs is complicated and to date, cost effective production has not been achieved.

Of the near-horizon battery technologies, SSLBs look to be the most promising for all-electric aircraft. The theoretical specific energy potential (2600 Wh/kg for Li-S SSLB) is not as high as aluminum-air batteries but their energy density is higher and SSLBs are rechargeable, safer and require fewer auxiliary systems on an aircraft.

The useful energy stored in a battery depends on the battery chemistry and the E-rate (or C-rate) of charging and discharging. For Li-ion batteries, the charge efficiency can be as high as 0.995 if charged and discharged slowly (≈1/32 C) but the energy efficiency $\eta_{battery} = E_{discharge}/E_{charge}$ is typically 0.985 or lower. In all-electric aircraft applications, the discharge E-rate varies over the course of the flight but it ranges up to 0.6E during takeoff and climb for aircraft designs that have an appreciable range. It should be noted that $\eta_{battery}$ can be much lower for battery packs used in hybrid designs where the discharge rates are high. The model implemented[15] for $\eta_{battery}$ in the current

study is based on characteristic power curves for Sanyo LI-18650 2.3 Ah Li-ion batteries with a technology factor F_{bat} applied to adjust for the expected efficiency increase (internal resistance of SSLB is lower than Li-ion) by SSLB technology:

$$\eta_{Battery} = (1 + C_1x + C_2x^2 + C_3y + C_4xy + C_5y^2)^{F_{bat}}$$

For the Sanyo LI-18650 2.3 Ah Li-ion cell as reported[15] $C_1 = -0.0612, C_2 = 0.0115, C_3 = -0.0781, C_4 = 0.0007873, C_5 = 0.0124$, F_{bat} = 1.0, *x* is the charging C-rate and *y* is the discharging C-rate. In the current study F_{bat} is set to 0.19. The original fit was created using *x*,*y* combinations up to 1.5C and is inaccurate at higher C-rates. The battery efficiency model was developed using measured data from a single cell. It is assumed that cell and pack efficiencies are equivalent. Furthermore, the particular battery chemistry can greatly impact the battery efficiency and so while the form of the above expression is probably applicable to other batteries, the numerical coefficients are not. Finally, because the General Aviation Synthesis Program (GASP) aircraft simulation is written in terms of power, we use the E-rate of discharging for *y* instead of the discharging C-rate in the battery efficiency expression (effectively this neglects battery voltage droop that is not explicitly modeled).

A key issue that needs to be addressed for MWh class battery packs is increasing cell capacity (Ah) to keep the total pack cell count to a manageable number. Shown in figure 4 is the cell count dependency on cell capacity for the 30.2 MWh battery required by one of the missions studied. The battery pack output voltage level is 1552 V_{dc} which is achieved by placing 388 four V_{dc} batteries in series. The total number of cells required is on the order of a million for the COTS batteries typically used in electric automobiles – a quantity that is two orders of magnitude too high to be practical. Therefore, battery cells that have a capacity of approximately 1000 Ah need to be developed to enable practical battery packs in the tens of MWhs.

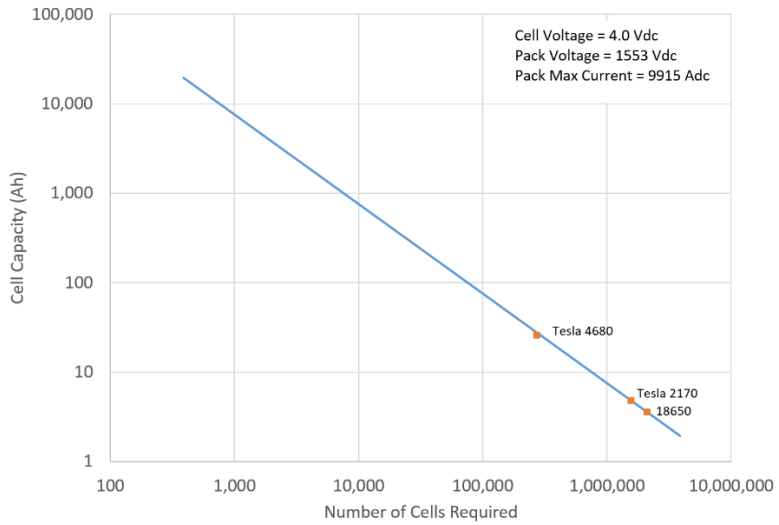

Figure 4. Total battery cell count for a 30.2 MWh pack consisting of 4 Vdc cells.

D. Propulsor Configuration

During this study we considered several propulsor configurations including ducted fans, single rotating open rotors (SR), counter rotating open rotors (CR) and configurations similar to the CFM RISE (SR with fixed stator). The goal is to maximize the propulsor efficiency while staying within the ICAO Annex 16, Chapter 4 aviation noise standard guidelines.

Early on in the study, we took a cursory look at a few ducted fan technologies such as the fan on the NK-93 and the LEAP 1B high-bypass turbofans, and compared them to open rotors like the Progress D-27, GE 36 and the CFM RISE configurations. It was decided that the blade tip loss reduction and increased safety benefits of ducted fans were outweighed by the drawbacks of higher nacelle weight, drag, and duct losses. Historically, the excessive noise

produced by the prop fans of the 1970s detracted from the fuel savings benefit of open rotors. Modern open rotors such as the Gen 1 A and Gen2A+B configurations studied during the CLEEN program[16] are projected to meet the post 2030 noise goal of 15-17 EPNdB cumulative margin to Chapter 4. During the CLEEN program, it was demonstrated that by clipping the aft rotor, proper inter-rotor spacing, and reducing the disk loading to less than 60 hp/ft^2, relatively low noise operation was achieved with little to no negative impact on rotor efficiency. Therefore, we chose to study a CFM RISE-like configuration and CR configuration.

Comparing the available rotor data at Mach 0.725 and 0.78 (i.e. B737-800 cruise Mach) shows that η_{net} is 0.2% higher at Mach 0.725. Decreases in SR and CR rotor efficiency at Mach above 0.725 has been seen in many datasets[17] yet there is a push to keep the Mach up (e.g. CFM RISE) in the belief that efficient and low noise rotors can be designed to operate at Mach 0.8. To be on the safe side, we have chosen 0.725 as the cruise Mach number even though the efficiency gain is small. Cruising at Mach 0.725 increases the DRM flight duration by 8 minutes over cruising at Mach 0.78 (to 2 hours and 15 minutes from taxi to landing).

For electrically propelled aircraft, the rotor is the largest source of inefficiency. Net propulsive efficiency η_{net} is the ratio of the useful power out of a propeller to the power supplied to the propeller in the presence of a nacelle which is often expressed in terms of a thrust coefficient ($C_T = T/\rho n^4 D^4$), power coefficient ($C_P = P/\rho n^3 D^5$) and an advance ratio ($J = V/n D$) as:

$$\eta_{net} = \frac{TV}{P_{shaft}} = \frac{C_T J}{C_P}$$

Propeller efficiency can be plotted versus a power coefficient divided by J^3 (a power loading parameter called PQAJ3) to further collapse the data.

$$PQAJ3 = \frac{C_p D^2}{A J^3}$$

Presented in figure 5 is a comparison of the net propulsive efficiency of a few open rotor configuration for which data is available in the open literature. The left graph shows a dataset published by Hamilton Standard Inc. of a SR prop fan[18] that was generated from wind tunnel tests of the SR-1 and SR-2 prop fans combined with modeling of advanced airfoils and blade planform shapes. The middle plot is of the F7/A7 CR rotor that was tested in the NASA Glenn 8×6 wind tunnel[19] and was the rotor on the GE36 engine that flew on an MD-80 in 1987. On the right is CR data[16] from tests of the Gen1A rotors (derived from the F31/A31 previously studied) that were tested in numerous facilities including the Glenn 8×6 as part of the CLEEN program. Of interest is that the peak net efficiency of these various rotor designs tops out at between 0.85 and 0.875. The purported six to eight percentage points efficiency advantage[17] of the CR over SR configurations (due to reduced residual swirl) diminishes at the lower power loading levels of modern designs (PQAJ3 < 0.1 during cruise). The implication is that the SR-stator RISE configuration may prove to be the best design in that it is lower weight and less complex than CR configurations yet the VP stator will remove some swirl imparted by the rotor and therefore the efficiency may be comparable to CR designs at least during cruise.

It should be noted that the Gen1A CR configuration maintains higher efficiency at the PQAJ3>0.1 levels encountered during climb in comparison to the older generation prop fan and F-7/A-7 CR designs. Another advantage of CR configurations is that the rotor diameter is smaller than SR designs producing the equivalent thrust and therefore the maximum tip speed is less for CR designs as is the per-rotor power loading.

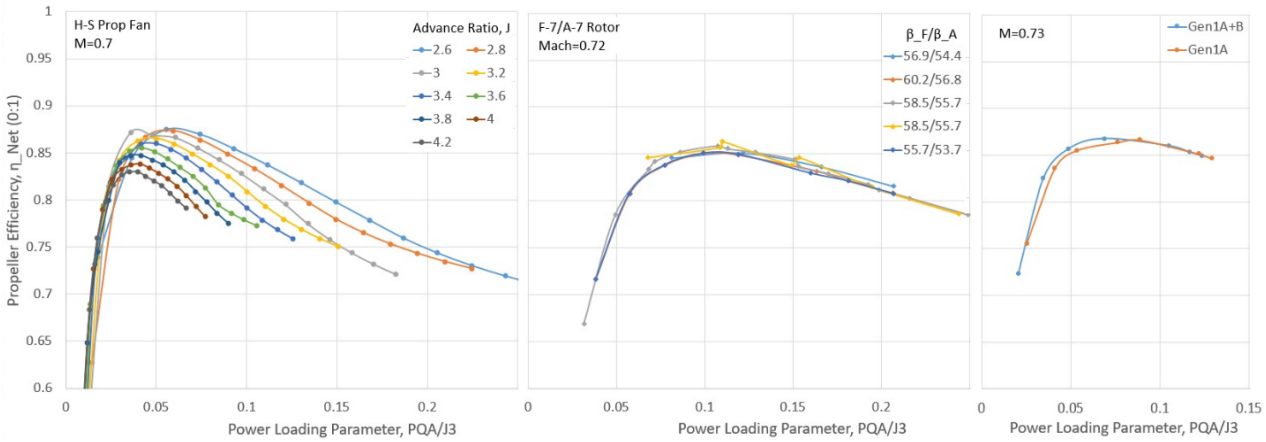

Figure 5. Propeller net efficiency versus power loading parameter for several rotor configurations.

Unfortunately, obtaining a sufficiently complete rotor performance data set of these configurations for simulation purposes was challenging (particularly for the CFM-RISE configuration[20], because this data has not been published in the open literature). As a result, we ended up implementing a low-disk-loading version of the Hamilton Standard prop fan in our simulations.

The propulsor configurations studied are shown in figure 6 (drawn approximately to scale). The configuration on the left is a VP prop-fan driven by four axial flux motors on a single direct-drive shaft, in the middle is a CFM RISE-like configuration with VP rotor and stator, and on the right is a variable pitch CR rotor, each rotor directly driven by two axial flux motors on concentric shafts. The drive shaft also turns a cooling pump that provides cooling to the motors, inverters and battery packs and an air compressor that slightly pressurizes the motor case to mitigate the arc flash potential (note that nacelle pressurization may not be necessary for the low voltage designs studied here). The forward rotor(s) are 14.0 ft. diameter. The permanent magnet axial flux motor details are described in the next section.

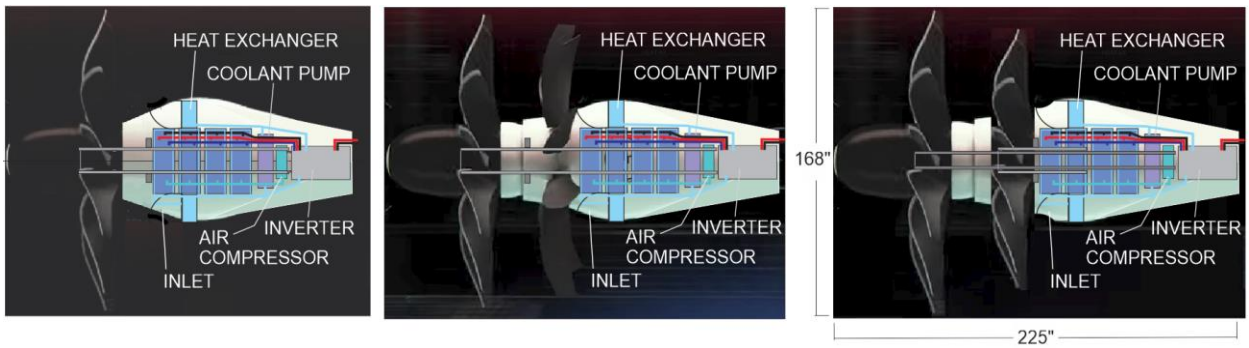

Figure 6. Open rotor propulsor configurations (left: SR, middle: SR with VP stator, right: CR).

E. Electric Motor Design

Virtually all of the motors under consideration for aviation propulsion are three-phase AC motors because these motors are more efficient and have higher specific power than single-phase motors. Motor topologies under consideration include permanent magnet machines (both radial and axial flux), induction machines, switched reluctance machines, wound-field synchronous machines, and synchronous reluctance machines[21]. In order to drive a propeller directly (i.e. without a gearbox) the motor must be capable of producing high torque at a relatively low rpm. Permanent magnet AC motors provide higher torque density than reluctance and induction motors but they are less fault tolerant. After consideration of these factors, we chose an axial flux permanent magnet machine. The main advantages of the axial flux topology is that it has higher power density than the radial flux counterpart and multiple motors can be stacked on a single shaft to produce high power and fit nicely within a nacelle.

The motor was designed using the MotorXP-AFM finite element software in consultation with MotorXP LLC (Chino, CA). The design process was started by specifying a motor outer diameter limit of 0.65 m and a maximum power of 3.2 MW. To minimize the possibility of arc flash at altitude, and to minimize the number of inverters needed in series, we attempted to keep the phase voltage as low as possible. As the design evolved, the number of slots and poles increased until we landed on a 40 pole 36 slot yokeless rotor-stator-rotor configuration with a Halbach array of GB48UH magnets (see figure 7) A commercially available motor of similar topology is shown in figure 8.

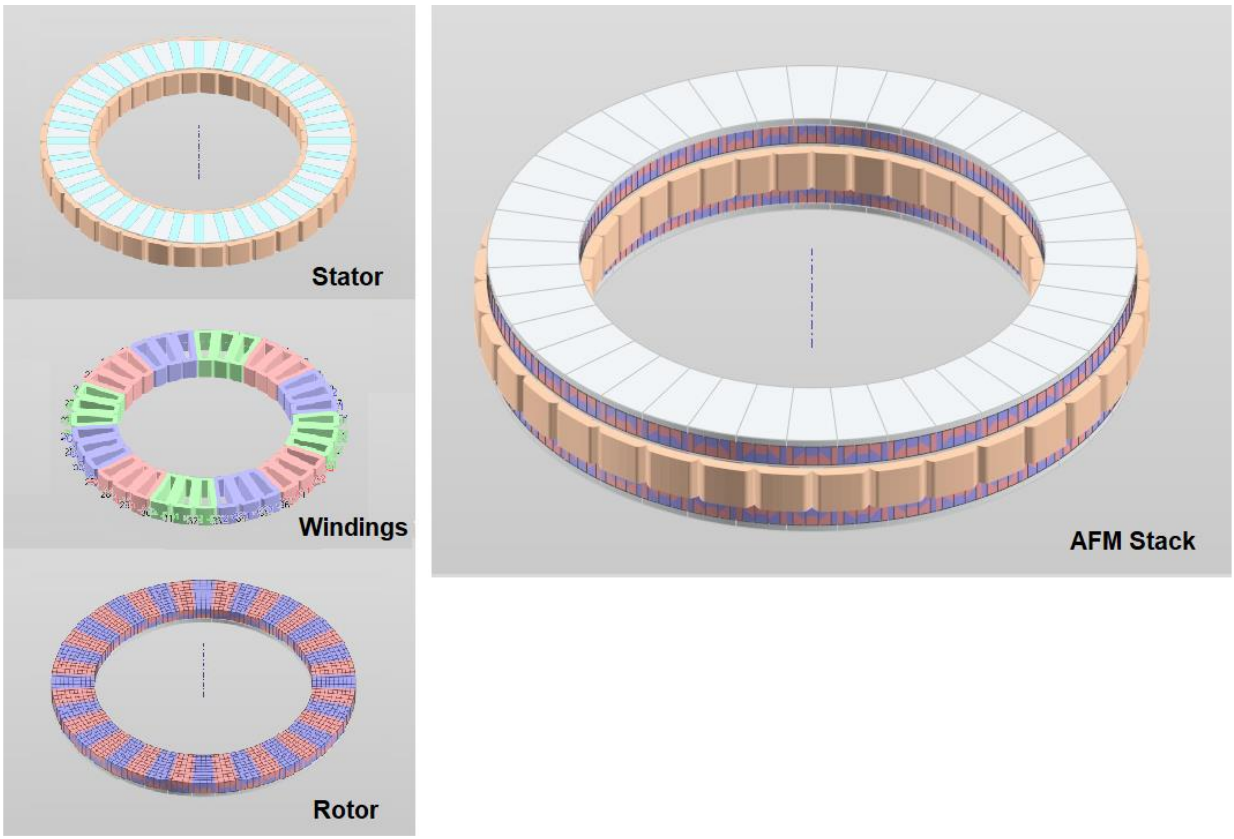

Figure 7. Conceptual 40P36S permanent magnet axial flux motor with peak input power of 3.2 MW.

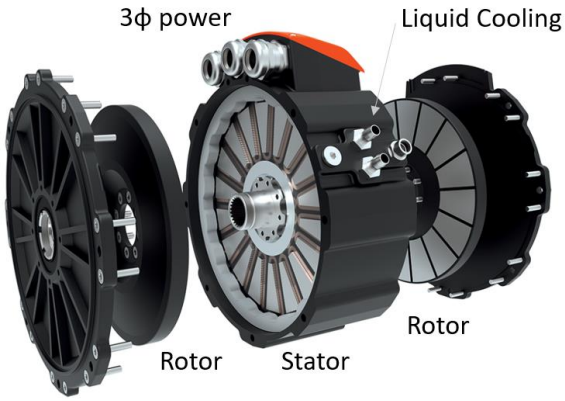

Figure 8. Axial-flux permanent magnet motor of similar topology (used with permission, Magnax Inc.).

The optimization capability of the MotorXP software was invoked at several points during the design process to

maximize motor efficiency and power factor, reduce the magnet weight and magnet eddy current losses.

A thermal analysis has not been performed on the motor because the liquid cooling system stator jacket has not been designed. A heat exchanger was sized based on the motor peak power losses during takeoff of 0.4 MW/nacelle assuming that the heat can be effectively transferred from the motor core to the working fluid that flows through the heat exchanger (see fig. 6). Manufacturability of the motor design has not been addressed but would likely be challenging and expensive because of the number of magnets and the challenge of how to reliably attach them to the rotor.

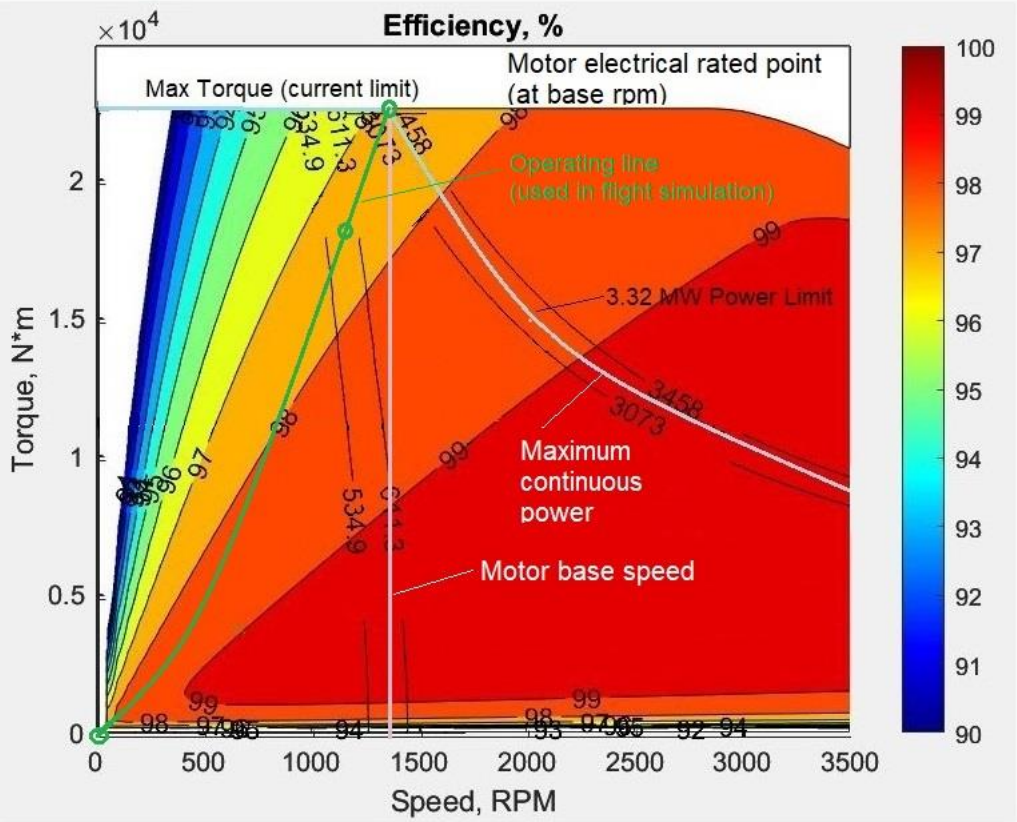

Figure 9. Predicted performance of the 3.2MW motor.

The predicted motor performance (for one of four motors/nacelle) is shown in figure 9 that was calculated using MotorXP's steady-state D-Q analysis. Included in the loss calculation are winding losses P_s, and first fundamental eddy current and hysteresis iron losses P_{iron}. This map does not include magnet losses and higher harmonics iron losses that were determined from a separate MotorXP magnetostatic finite element analysis at key operating points during climb and cruise. Magnet losses reduce efficiency ≈0.3% and higher harmonic iron losses are negligible. In the aircraft simulations described in a later section, the motor efficiency is calculated as:

$$\eta_{motor} = \frac{P_{shaft}}{P_{shaft} + P_s + P_{iron} + P_{magnet} + P_{other}}$$

The winding temperature was set to 60^o C based on temperature limits of the GB48UH neodymium-iron-boron magnets.

The maximum torque and power limits shown in figure 9 are electrical limits per motor. The continuous operating limits were set to be equivalent to 98% of the electrical limits. The assumption is that the liquid cooling system will be capable of maintaining the coil and magnet temperature to 60^o C or less when operating in the continuous regime.

Total torque provided and total input power required are four times that shown in the figure per nacelle. The basic performance specifications of the motor are listed in Table 1.

Table 1. Predicted motor electrical specifications for four motors in each nacelle.

Motors per nacelle	4
Maximum input power	3.32×4=13.28 MW
Maximum torque	22.5×4=90 kNm
Motor base speed	1350 rpm
Maximum shaft power	22,500*(2π*1350/60)×4= 12.7 MW (or 17,000 hp)
Nominal DRM max phase current required	1056×4=4224A_{ac}
Phase voltage required	Up to 634 V_{ac} (during takeoff and climb)

F. Power Electronics

A simplified diagram of the power system is shown in figure 10. The onboard portion of the system consists of a battery management subsystem, and battery packs and inverters in series and parallel.

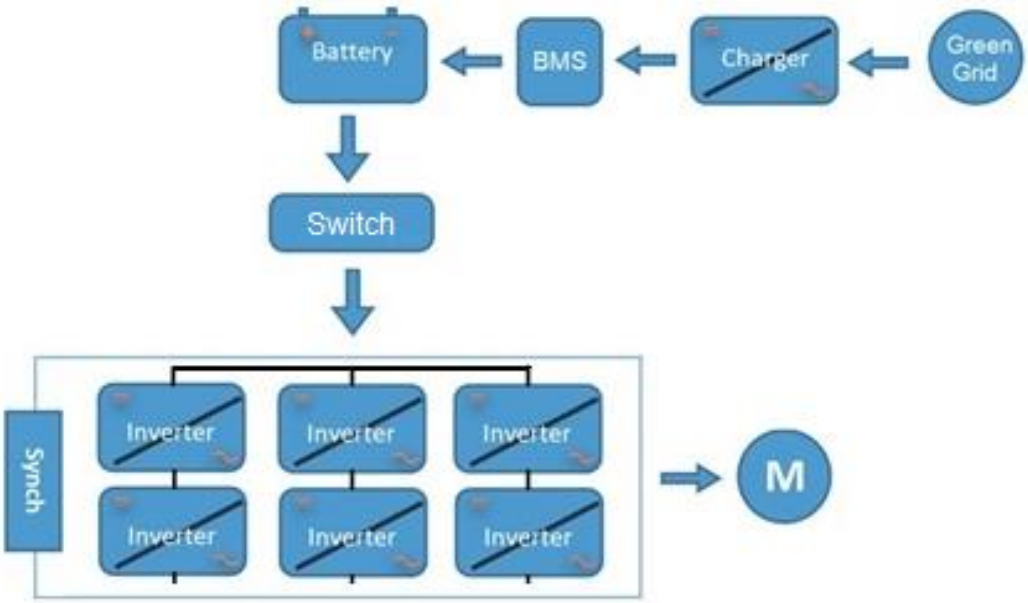

Figure 10. Simplified schematic of the aircraft power system.

Inverters that convert DC power from batteries to three-phase AC power to drive permanent magnet motors are an important component in an all-electric powertrain. Inverters approximate sinusoidal AC by switching semiconductor devices at frequencies of 10 kHz or so. Inverters based on Silicon Carbide (SiC) MOSFET technology enable higher switching power and as well as high switching speeds and low power losses in a compact package in comparison to inverters based on other common technologies such as IGBT and Si semiconductor devices.

Shown in figure 11 is the specific power and power density of commercially available three-phase DC to AC traction inverters. Of the inverters shown, only the Magnix inverter is specifically designed for aviation applications (others are traction inverters for automotive use). The WolfSpeed Inc. model CRD600DA12E-XM3 inverter uses SiC technology with specific power of 62 kVA/kg and power density of 72400 kVA/m^3 and is roughly twice as power dense as its nearest competitor (the lower power density units typically use the less expensive IGBT technology). Scaling the power from 0.6 MW (for the CRD600) to the DRM baseline design (i.e design with battery SE of 1330 Wh/kg) peak power of roughly 17 MW required during takeoff would result in an inverter with mass of 262 kg (0.43% of the aircraft takeoff mass) and volume of 0.23 m^3. Often multiple inverter circuits are packaged in a single box

because the individual MOSFET circuits are power, voltage and current limited. To achieve the individual motor maximum phase voltage of 634 V_{rms} and phase current of 1024 A_{rms} the baseline design requires 4 SiC inverters in parallel per motor (CRD600 or equivalent) and possibly inverters in series to slightly boost the AC voltage. A quantity of 32 weighing 310 kg in total were bookkept for the current design.

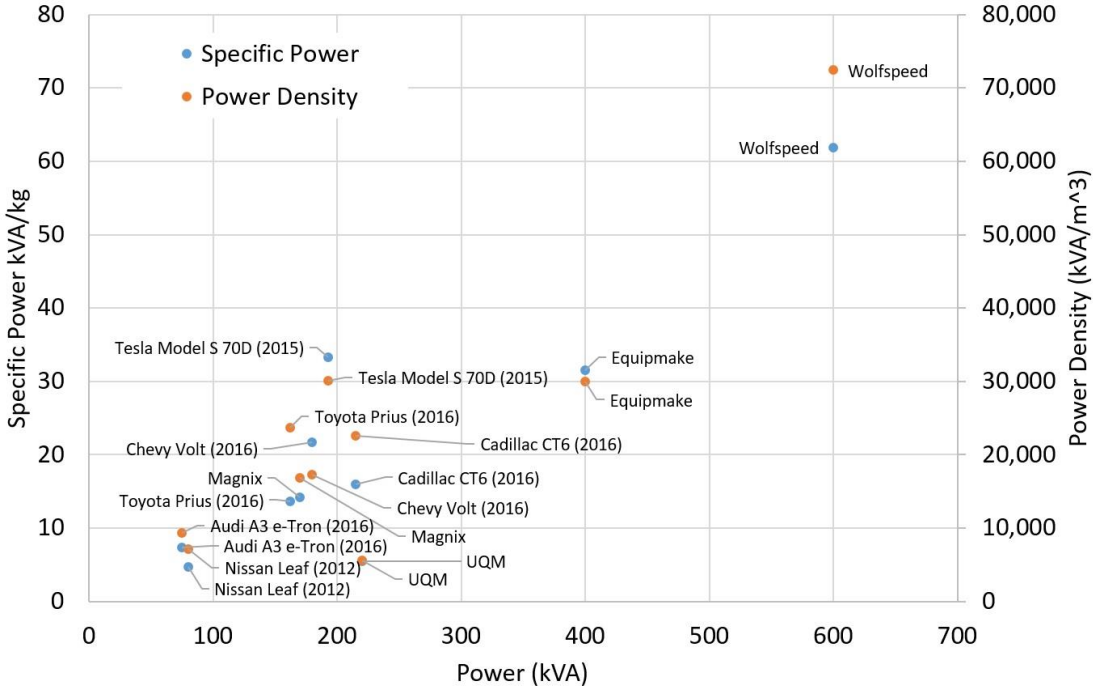

Figure 11. Specific power and power density of various commercially available inverters.

The efficiency of well-designed inverters can be quite high over a range of loads depending on the inverter technology (see figure 12). Over most of the simulated DRM $\eta_{inverter} \approx 0.995$ for the SiC inverter except during descent when the inverter efficiency decreased to 0.20 because the inverter load ratio was less than 5%. This problem was addressed by adding switches (solid state or contactor) to tailor the number of inverters (in parallel) to the motor current demand. Adding switches increased the descent inverter efficiency to about the same level as during cruise.

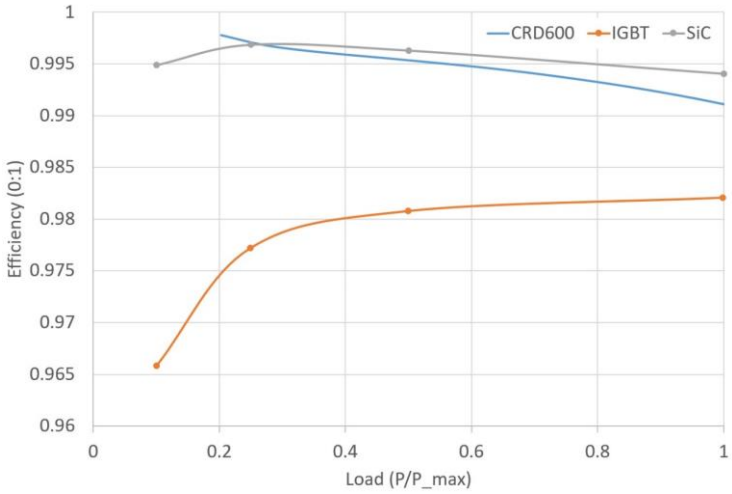

Figure 12. Efficiency of commercially available inverters IGBT and SiC data from ref. 22, CRD600 data from ref. 23.

The inverter efficiency was modeled by fitting a curve to the SiC data of figure 12 and then raising the efficiency of a single inverter stage to the power of the number of stages in series.

$$\eta_{inv} = \left(-0.0085{P_r}^2 + 0.0079P_r + 0.9947\right)^{N_s} \quad \text{for } 0.1 < P_r < 1.0$$
$$\eta_{inv} = (0.09954P_r)^{N_s} \quad \text{for } 0.0 < P_r < 0.1$$

Where $P_r = P_{inv}/P_{inv\ max}$ is the inverter load and N_s is the number of inverter stages in series. For inverter loading less than 10% the efficiency curves are extrapolated to zero.

Inverter power output is dependent on operating temperature and so inverters are often designed with coolant loops. For example, the CRD600 requires 24 L/min of water at 20 C to deliver its rated 0.6 MW of power. In aircraft applications, the heat generated by inverters (and batteries and motors) is ultimately rejected to the airstream and so a heat exchanger and coolant pumping system is required.

G. Cabling Losses

The cabling losses are surprisingly high for designs where the inverters, batteries and motors are not in close proximity to each other ($\eta_{cable} \approx 0.978$ for a comparable design with fuselage-mounted inverters). AC cabling losses are particularly problematic because of the tendency of AC currents to flow along the conductor outer edge (rather than evenly distributed as in DC cabling). To minimize cabling losses and weight, cabling runs should be a short as possible. Placing the batteries in the wings and inverters in the motor nacelle would be ideal because the AC and DC cabling runs would be short and the battery weight would provide wing-bending-moment relief but the batteries would be inaccessible for maintenance, which may not be practical. On the other hand, inverters could be placed in the motor nacelle without greatly impacting the nacelle volume as shown to scale in figure 13. Close coupling the inverter with the motor configuration increases η_{cable} to 0.996 and reduces the cabling weight by approximately 50% compared to a design with inverters in the fuselage. Furthermore, the inverters are close to the cooling source thus simplifying the cooling system design.

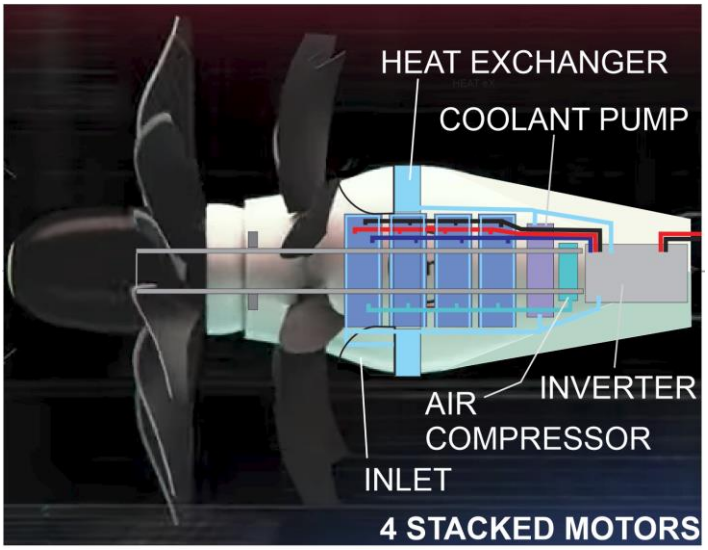

Figure 13. Nacelle with inverter.

Each motor is assumed to have its own separate AC cabling run from the inverter bank. The desired motor input phase rms voltage V_{ph}, current I_{ph} and PF are known from motor performance predictions and the 3-phase motor input power is $P_{mtr\_in} = 3V_{ph}I_{ph}PF$. The model for the AC cable efficiency η_{ac_cable} is based on determining the voltage drop caused by the AC cable effective impedance:

$$\eta_{ac\_cable} = \frac{P_{mtr\_in}}{P_{inv\_out}} = \frac{3V_{ph}I_{ph}PF}{P_{inv\_out}} = \frac{V_{ph}}{V_{ph} + V_{D\_ac\_cable}}$$

Where: $$V_{D\_ac\_cable} = I_{ph}\left[\frac{10.090[1+0.00323(T_{ac\_w}-75)]}{D_{ac\_cmil}}\cos\phi + 0.000123{D_{ac\_cmil}}^{-0.088}\sin\phi\right]\left(\frac{f}{60}\right)L_{ac\_cond}$$

In the equations above, the motor power factor is $PF = \cos\phi$ and $V_{D\_ac\_cable}$ is the cable rms voltage drop over an average length $L_{ac\ cond}$ (ft.) of copper wire at temperature $T_{ac\ w}$ (Fahrenheit) and $D_{ac\ cmil}$ is the AC conductor cross-sectional area in circular mils. Note that cable effective impedance is proportional to frequency. The $f/60$ factor is the inverter fundamental output frequency $f = rpm_{motor}N_p/(2 \times 60)$ to 60 Hz ratio that models higher frequency when using 60 Hz cable specifications.

The DC cabling efficiency $\eta_{dc\ cable}$ for the cable between the battery and the inverter, written in terms of the motor input AC phase voltage and current is determined similarly:

$$\eta_{dc\_cable} = \frac{P_{inv\_in}}{P_{bat\_out}} = \frac{V_{ph} + V_{D\_ac\_cable}}{\left(V_{ph} + V_{D\_ac\_cable} + G\ V_{D\_dc\_cable}\right)}$$

Where: $$V_{D\_dc\_cable} = 6\left[\frac{G\ I_{ph}PF\ N_{motors}}{\eta_{ac\_cable}\eta_{inv}}\right]\left[\frac{10.090[1+0.00323(T_{dc\_w}-75)]}{N_{dc\_cable}D_{dc\_cmil}}\right]L_{dc\_cond}$$

In the above expression, N_{dc_cable} is the total number of DC conductor pairs and V_{D_dc} is the DC voltage drop for a copper conductor pair of conductor cross-sectional area D_{dc_cmil} and average length L_{dc_cond} (ft). The inverter output rms voltage is $V_{ac\ inv\ out} = G\ V_{dc\_inv\_in}$ and G= 0.4082 is a typical gain for a space-vector pulse-width-modulated DC to three-phase AC inverter.

H. Aircraft Configuration

Pulling it all together, the design is shown in figure 14. The airframe is similar in many respects to the low-wing B737-800 with winglets except with four battery packs and mid-wing mounted nacelles that house four motors each with inverters. The rotor-tip ground clearance is 18.9 inches (the same as the minimum nacelle ground clearance on a B737-800).

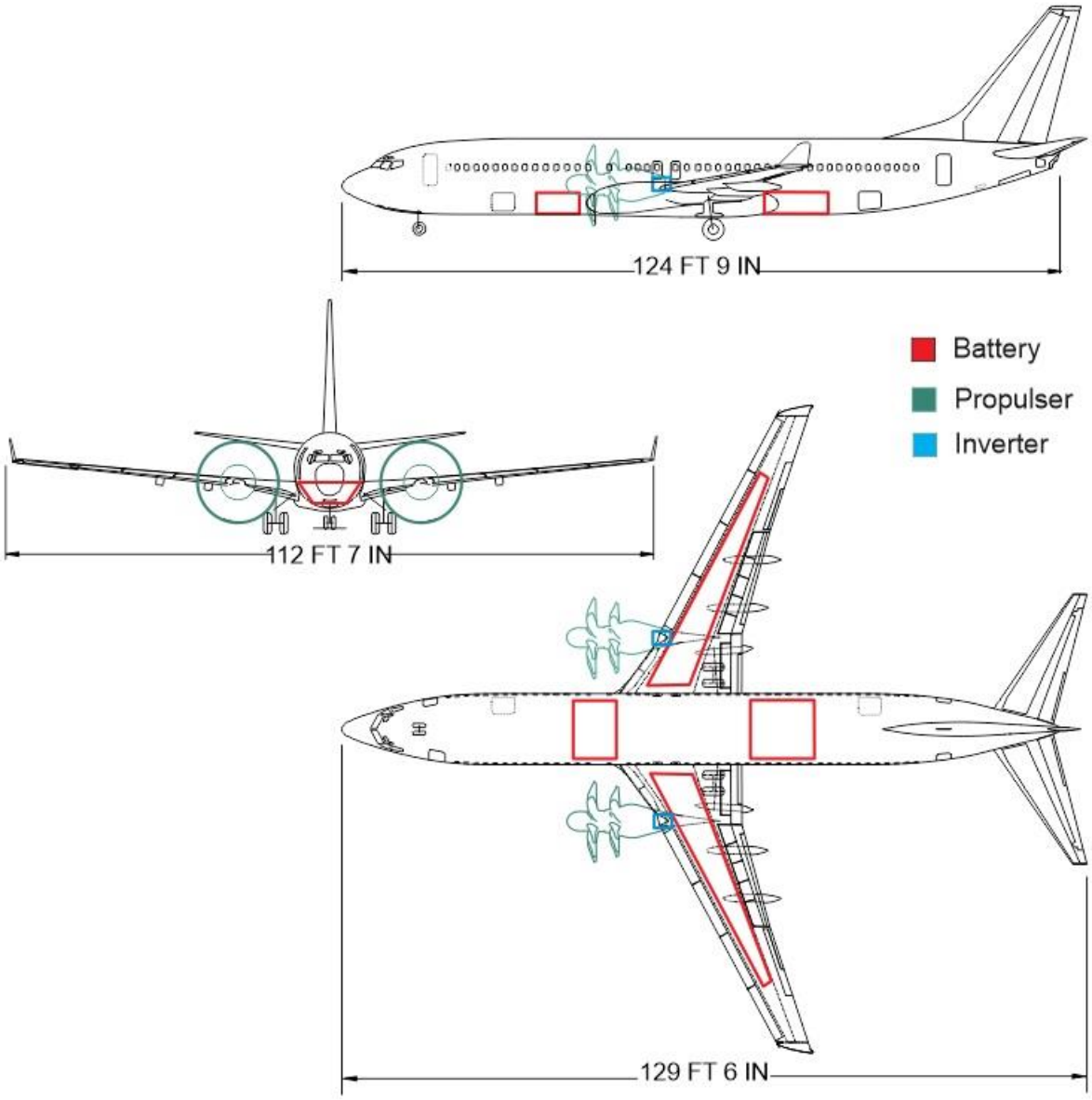

Figure 14. Notional 150-pax all-electric aircraft.

Table 2. Summary of the baseline 150 pax all-electric design stats for the DRM flight.

Item	Quantity	Remarks
Pax	150	195 lb each including carryon
Range (NM)	840	
TO weight (lbs)	150,000	
Operating empty weight (lbs)	120,750	90,710 lbs for B737-800
Battery pack weight (lbs)	49,392	
Battery pack specific energy (Wh/kg)	1330	
Battery reserve energy (%)	24.5	
Cruise L/D	17.75	with winglets
Cruise Mach	0.725	
Cruise wing loading (psf)	111.3	
Sea level shp/nacelle	9622	with all motors during takeoff
Motor cruise rpm	1187	
Takeoff rotor power loading (SHP/ft^2)	62.5	
Maximum rotor tip speed (ft/s)	990	SR speed is too high for low noise (but lower speed expected for CR design)

I. Simulation Results

The computer code GASP[24] that performs preliminary design of fixed-wing aircraft was used to study the flight performance and design sensitivities of an all-electric 150 pax configuration. GASP has been in use and regularly improved since the mid-1970s. The program uses a combination of analytical models and empiricism to model the weight, aerodynamics and propulsion of a user specified aircraft configuration. Essentially, the program iterates on the aircraft geometry and propulsion system size until the design achieves a desired DRM flight range within a set of constraints. The user inputs motor and propeller performance data and the program matches the propeller to the motor. In the hands of an experienced user, GASP can predict flight range and fuel (or energy consumption) to within ±5%.

To generate the results, we started with a GASP model of a B737-800 and reduced the wing, fuselage, horizontal and vertical tail structural weights by 21% to account for advanced tube and wing composite construction techniques (saving 8157 lbs). Belly cargo was eliminated (no luggage, only carryon). The original seats were replaced with lightweight versions weighing 29 lbs each. The turbofan engines were replaced with mid-wing mounted electric motor driven rotors (see fig. 13) and battery packs were added to the wings and fuselage as shown in figure 14. When running the simulation, the battery energy density was adjusted until we achieved the DRM goal of 840 NM plus reserves. We did not alter the aerodynamic performance of the B737-800 except for the differences associated with the nacelle placement and size. Note that the landing mass is 150,000 lbs which is slightly heavier than the B737-800 maximum landing weight of 133,800 lbs but lighter than the B737-800 maximum takeoff weight of 155,000 lbs (landing gear will need to be strengthened).

Presented is figure 15 is the flight velocity and altitude time history along with the battery power and energy required for the simulated 150 pax 840 NM all-electric DRM. Not shown is the reserve mission (see fig. 2) that requires an additional 7.1 MWh of energy (i.e. 24.5% of the total 28.8 MWh initially stored onboard). Furthermore, substantial power is required at the end of the reserve mission for thrust reversal during landing which might challenge a nearly depleted battery.

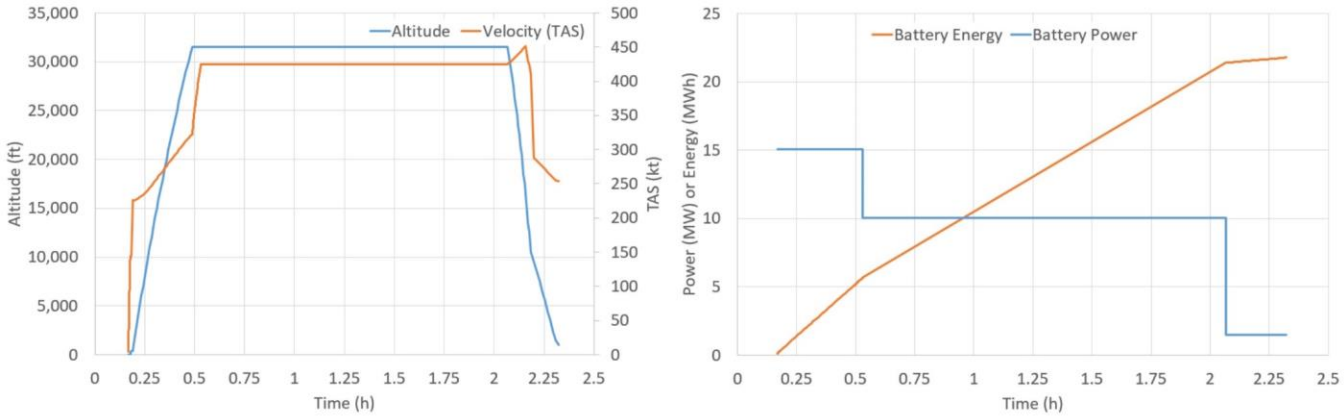

Figure 15. Velocity and altitude (left) and battery power and energy (right) time histories of the 840 NM DRM.

The efficiency time history of the flight is presented in figure 16. During takeoff, the total efficiency (η_{total}) increases to about 78% and then it dips to about 72% during climb primarily because of the rotor is operating at reduced efficiency. During cruise, the total efficiency is 82% and during descent, the total efficiency decreases dramatically caused by a precipitous drop in rotor efficiency. The inverter efficiency remains high during descent even though the power is greatly reduced because three of the four inverters serving each motor have been switched off thereby increasing the loading on the remaining inverter to approximately 17%, which resulted in an inverter efficiency of 99.2%.

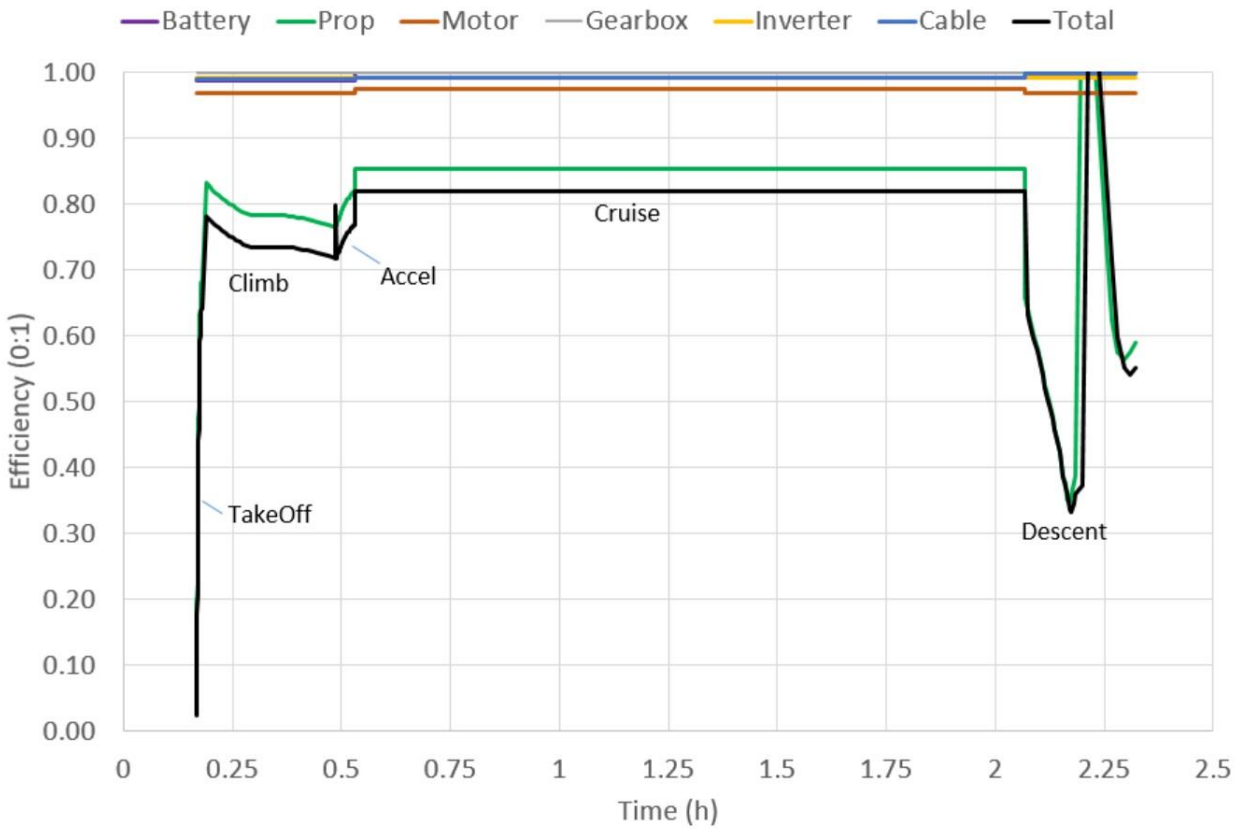

Figure 16. Efficiency time history.

Based on the rotor performance data shown in figure 5, it should be possible to increase the rotor efficiency by a percentage point or so by optimizing the rotor design and motor matching. This process was not undertaken because increasing the efficiency of the prop fan would likely result in excessive rotor tip speeds and increased noise. Modern rotor CR designs such as the GEN 2A show a rotor net efficiency level of approximately 0.845 at design power[16] and noise levels of 15-17 EPNdB cumulative margin relative to CAEP Chapter 4 (but not enough publically available data for simulation purposes).

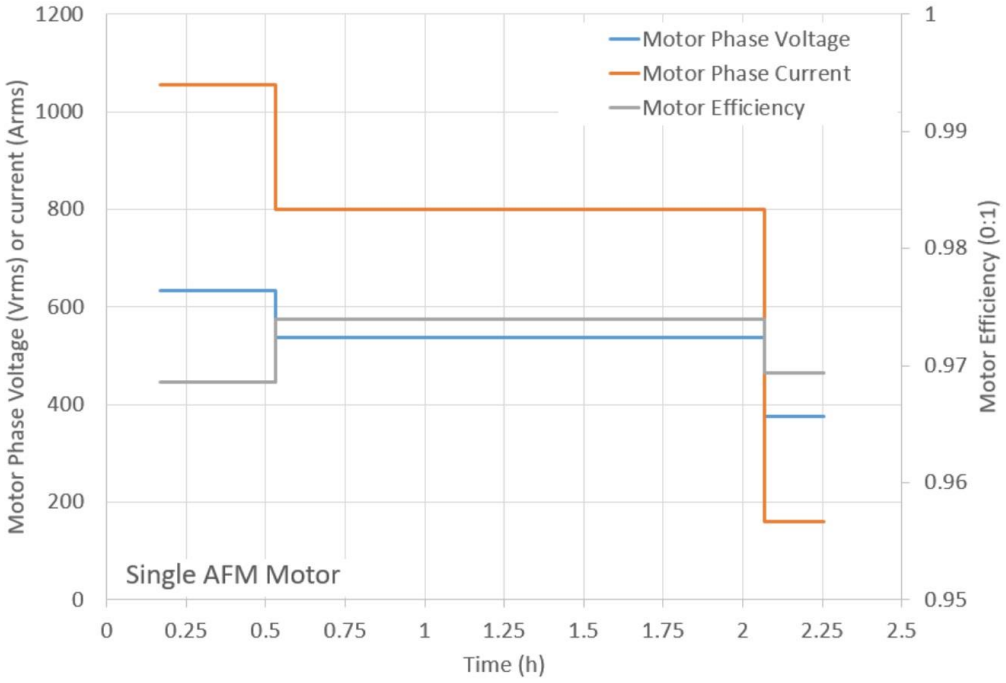

Figure 17. Single motor phase voltage, current and efficiency time history.

The phase voltage of the axial flux motors is comparatively low for a power plant with aggregate of 13,680 SLS shaft horsepower per nacelle as shown in figure 17. A design trade was made to gain power through current rather than voltage (to minimize the arc flash potential) at the expense of cabling weight. The estimated total cabling weight is 1306 lbs which is appreciable but not a show stopper.

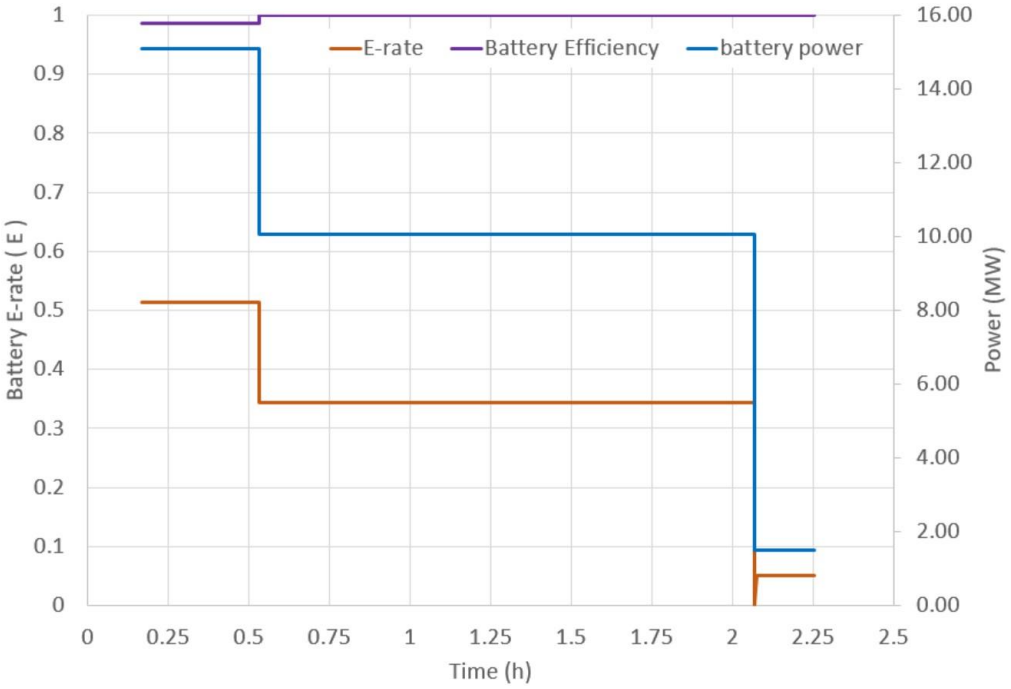

Figure 18. Battery E-rate time history.

As mentioned previously, the battery efficiency depends on the discharge rate. Figure 18 shows that the battery E-rate is approximately 0.52 ($\eta_{bat} = 0.987$) during takeoff and climb and the E-rate decreases to 0.34 during cruise and 0.05 during descent. In this simulation, the battery was charged at 0.5C and its efficiency is above 98% for the whole flight. The relatively high battery efficiency during flight is a result of implementing SSLBs that have low internal resistance. If the SSLBs were replaced with the Li-ion batteries studied in ref. 13, η_{bat} would be 0.932 during takeoff and climb for an equivalent size pack.

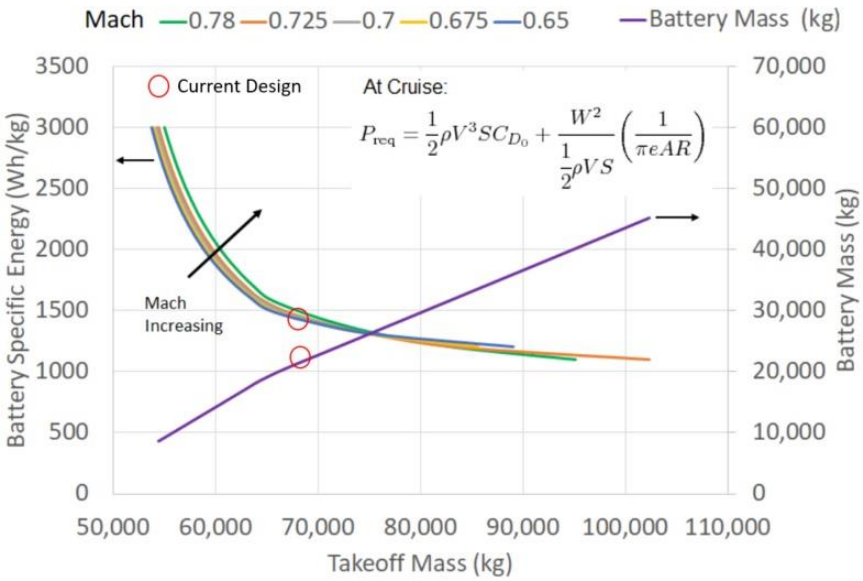

Figure 19. Battery specific energy trend for 150 pax, 840 NM mission.

The results shown so far are for a battery specific energy level of 1330 Wh/kg which is likely to be a post 2070 level (see fig.3) and may not be achievable even then. Shown in fig. 19 is the aircraft battery specific energy versus takeoff mass for the 840 NM DRM (based on a simplified analysis using the cruise power equation shown in the

figure). This analysis shows that for the level of technology described in this paper, the takeoff mass increases at a high rate for battery specific energy levels less than approximately 1300 Wh/kg. So, to have an appreciable impact on GHG without significant changes in airspace operations (e.g. replacing longer flights with multiple short flights), developing high specific energy storage is essential.

IV. Conclusions

Presented in this paper is the conceptual design of a 150 pax all-electric aircraft with a 840 NM range that, if implemented at scale, could lead to a flight-related GHG reduction of 29% (relative to 2019) provided the batteries are charged with green electricity. The battery pack specific energy level implemented in the simulations is 1330 Wh/kg-- a stretch goal for what may be possible in the future.

Wherever possible we have tried to eke out as much efficiency as reasonable, but the design presented here has not been optimized. Nevertheless, the process of creating this conceptual design led to some important realizations:

1.) The minimum battery energy density required to realize a 150 pax aircraft with a range of 840 NM is approximately 1330 Wh/kg. Further reductions in required minimum battery energy density down to about 1200 Wh/kg could be achieved through optimizing the design for a cruise Mach number of 0.625. This would add 18 minutes to the 840 NM flight time.

2.) The average total energy efficiency of the DRM flight is 0.78, which is approximately twice that of the equivalent turbofan powered flight.

3.) Mounting the inverters in the nacelle increases the AC cabling efficiency and therefore total efficiency by 1 to 2% and decreases cabling weight significantly over that of designs with fuselage mounted inverters.

4.) Use of SSLBs is predicted to be up to 5% more efficient in comparison to Li-ion batteries because SSLBs have lower internal resistance along with several other beneficial features including high energy density, fast charging, long cycle life, reduced heat, and most importantly improved safety.

5.) Silicon carbide-based inverters are 1.5% more efficient and twice as gravimetrically and volumetrically dense as competing technologies.

6.) Multiple inverters in parallel may be required for large all-electric aircraft. If so, it is important to keep the inverter loading above 10% for reasonable inverter efficiency. The can be achieved during the low power flight phases (e.g. descent) by switching lightly loaded inverters out of the circuit.

7.) Unlike gas turbines, electric motors can be designed to efficiently produce torque at shaft rotation rates that match rotor advance ratios near peak rotor efficiency during cruise and therefore a gearbox is not required.

8.) The axial-flux permanent magnet motor design is lightweight, compact, powerful and efficient over a range of shaft speeds. The predicted motor cruise efficiency is 0.974.

9.) Modern counter rotating rotor configurations maintain higher efficiency over a broader range of power loading in comparison to older generation technology. It is not clear that the higher rotor efficiency will lead to a better overall aircraft design because of the added weight and complexity associated with the CR mechanisms.

10.) The stacked motor design produces up to 17,000 SLS shaft hp motor per nacelle (although only 9622 is required by the DRM with all motors operational). During the DRM simulation, the maximum motor phase voltage is 634 Vrms which is roughly half of the breakdown voltage at 40,000 ft and therefore the potential for arcing within the motor is low. This is seen as a key advantage of a low voltage high current motor design.

11.) The maximum rotor tip speed encountered during the DRM is 990 ft/s and the maximum rotor power loading is 62.5 shp/ft^2. These numbers are borderline too high to meet future noise guidelines. Implementation of the CR

configuration should result in lower tip speed, decreased power loading and increased average rotor efficiency. Furthermore, electrically driven rotors do not produce core noise which is a substantial contributor to the total noise produced by turbofan driven rotors.

The efficiency gains mentioned above translate directly to total efficiency gains and therefore to net power and energy savings. Additional efficiency gains could be achieved through implementation of advanced aerodynamic technology.

Here is a list of the technology gaps identified in this all-electric aircraft design study.

1.) Development of safe high-power battery packs with specific energy of at least 1330 Whr/kg would open up the design space and lead to significantly more capable all-electric aircraft.

2.) Battery cell power capacity needs to be increased to around 1000Ah per cell to make MW class battery pack practical for use in electric aviation.

3.) Axial flux cooling jacket design should be explored to determine if high-power compact designs are achievable in practice. Motor cooling was not addressed in the current study.

Acknowledgement

This work is sponsored by NASA's Aeronautics Research Mission Directorate (ARMD) and was carried out under the Electrified Powertrain Flight Demonstration (EPFD) project. Access to annual air traffic data is provided by the Sherlock air traffic data warehouse hosted at NASA Ames.

References

[1] Federal Aviation Administration. (2021) *United States 2021 Aviation Climate Action Plan* Washington, D.C. GPO https://www.faa.gov/sites/faa.gov/files/2021-11/Aviation_Climate_Action_Plan.pdf
[2] Melton, J., Go, S., Zilliac, G., Zhang, B., "Greenhouse Gas Emission Estimations for 2016–2020 using the Sherlock Air Traffic Data Warehouse," NASA/TM-20220007609, Aug., 2022.
[3] Bradley M. K., and Droney, C. K., "Subsonic Ultra Green Aircraft Research:Phase II – Volume II – Hybrid Electric Design Exploration," NASA NASA/CR–2015-218704/Volume II, 2015.
[4] Jansen, R., et al., "Subsonic Single Aft Engine (SUSAN) Transport Aircraft Concept and Trade Space Exploration," AIAA SciTech Forum, January 3-7, 2022, San Diego, CA.
[5] https://caafi.org/focus_areas/docs/US_WasteFeedstockPotential.pdf
[6] World Economic Forum, "Clean Skies for Tomorrow Sustainable Aviation Fuels as a Pathway to Net-Zero Aviation," Insight Report, November 2020.
[7] Stückl, S., van Toor, J., and Lobentanzer, H., "VoltAir - The All Electric Propulsion Concept Platform –A Vision for Atmospheric Friendly Flight," ICAS, Brisbane Australia, 2012.
[8] Hornung, M., Askin T., Isikveren, A., Cole, M., and Sizmann, A., "Ce-Liner - Case Study for eMobility in Air Transportation," AIAA 2013-4302, Los Angles, 2013.
[9] Wolleswinkel, R., de Vries, R., Hoogreef, M., and Vos, R., "A New Perspective on Battery-Electric Aviation, Part I: Reassessment of Achievable Range," AIAA SciTech Forum, Orlando, FL, 2024.
[10] de Vries, R., Wolleswinkel, R., Hoogreef, M., and Vos, R., "A New Perspective on Battery-Electric Aviation, Part II: Conceptual Design of a 90-Seater," AIAA SciTech Forum, Orlando, FL, 2024.
[11] Go, S., Melton, J., Jiang, X., Zilliac, G., "Estimations of Aircraft and Airport Domestic Greenhouse Gas Emissions from 2016-2021," AIAA EATS conference, San Diego, 2023.
[12] Blake Tiede, B., O'Meara, C., Jansen, R., "Battery Key Performance Projections based on Historical Trends and Chemistries," 2022 EATS Conference, Anaheim, 2022.
[13] Viggiano et al. "Solid-state Architecture Batteries for Enhanced Rechargeability and Safety for Electric Aircraft," Prime 2020 Presentation. https://ntrs.nasa.gov/api/citations/20205008150/downloads/Rocco%20Viggiano%20%E2%80%93%20CAS%20SABERS%20PRiME%202020%20Presentation%20%E2%80%93%2020205008150.pdf

[14] Ye, L., Li, X., “A Dynamic Stability Design Strategy for Lithium Metal Solid State Batteries,” *Nature* 593, 218–222 (2021).
[15] M. Toman, M., Cipin, R., Cervinka, D., Vorel, P., Prochazka, P., “Li-ion Battery Charging Efficiency,” ECS Transactions, 74 (1) 37-43 (2016).
[16] Khalid, S.A., Lurie, D., Breeze-Stringfellow, A., Wood, T., Ramakrishnan, K., Paliath, U., Wojno, J., Janardan, B., Goerig, T., Opalski, A., Barrett, J., “Open Rotor Engine Aeroacoustic Technology Final Report,” Continuous Lower Energy, Emissions and Noise (CLEEN) Program, General Electric, FAA, 2013.
[17] Hager, Roy D., and Vrabel, Deborah, “Advanced Turboprop Project”, NASA SP–495, 1988.
[18] Baum, J.A., Dumais, P.J., Mayo, M.G., Metzger, F.B., Shenkman, A.M., and Walker, G.G., "Prop-Fan Data Support Study Technical Report," NASA CR-152141, 1978.
[19] Hoff, G.E. et al., “Experimental Performance and Acoustic Investigation of Modern, Counterrotating Blade Concepts,” NASA-CR-185158, 1990.
[20] Norris, G., “CFM RISE Open Fan Passes Conceptual Review Milestone,” AW&ST, November 13 2023.
[21] Zhang, X., Bowman, C. L., O'Connell, T. C., Haran, K. S., “Large Electric Machines for Aircraft Electric Propulsion,” IET Electric Power Applications, 2018, p. 767-779.
[22] Chakravarthy, B.K. and Sree Lakshmi, G., “Power Savings with all SiC Inverter in Electric Traction Applications,” E3S Web of Conferences SeFet 87, 2019.
[23] Feutado, M., Martin, D., McNutt, T., “Silicon Carbide Modules Unlock Higher Power Density in Motor Drives,” Jan 04, 2022.
[24] "GASP - General Aviation Synthesis Program", Vol. 1- Main Program Vol. 2- Geometry, Vol. 3 - Aerodynamics, Vol. 4 - Propulsion, Vol. 5 - Weight and Balance, Vol. 6 - Performance, Vol. 7 - Economics. NASA CR-152303, January 1978.